

## Robust Fermi-Surface Morphology of CeRhIn<sub>5</sub> across the Putative Field-Induced Quantum Critical Point

S. Mishra<sup>1</sup>, J. Hornung<sup>2,3</sup>, M. Raba<sup>1,†</sup>, J. Klotz<sup>2</sup>, T. Förster<sup>2</sup>, H. Harima<sup>4</sup>, D. Aoki<sup>5</sup>,  
J. Wosnitzer<sup>2,3</sup>, A. McCollam<sup>6</sup>, and I. Sheikin<sup>1,\*</sup>

<sup>1</sup>Laboratoire National des Champs Magnétiques Intenses (LNCMI-EMFL), CNRS, UGA, 38042 Grenoble, France

<sup>2</sup>Hochfeld-Magnetlabor Dresden (HLD-EMFL) and Würzburg-Dresden Cluster of Excellence ct.qmat, Helmholtz-Zentrum Dresden-Rossendorf, 01328 Dresden, Germany

<sup>3</sup>Institut für Festkörper- und Materialphysik, TU Dresden, 01062 Dresden, Germany

<sup>4</sup>Graduate School of Science, Kobe University, Kobe 657-8501, Japan

<sup>5</sup>Institute for Materials Research, Tohoku University, Oarai, Ibaraki, 311-1313, Japan

<sup>6</sup>High Field Magnet Laboratory (HFML-EMFL), Radboud University, 6525 ED Nijmegen, The Netherlands

 (Received 11 May 2020; revised 18 November 2020; accepted 15 December 2020; published 6 January 2021)

We report a comprehensive de Haas–van Alphen (dHvA) study of the heavy-fermion material CeRhIn<sub>5</sub> in magnetic fields up to 70 T. Several dHvA frequencies gradually emerge at high fields as a result of magnetic breakdown. Among them is the thermodynamically important  $\beta_1$  branch, which has not been observed so far. Comparison of our angle-dependent dHvA spectra with those of the non-4*f* compound LaRhIn<sub>5</sub> and with band-structure calculations evidences that the Ce 4*f* electrons in CeRhIn<sub>5</sub> remain localized over the whole field range. This rules out any significant Fermi-surface reconstruction, either at the suggested nematic phase transition at  $B^* \approx 30$  T or at the putative quantum critical point at  $B_c \approx 50$  T. Our results rather demonstrate the robustness of the Fermi surface and the localized nature of the 4*f* electrons inside and outside of the antiferromagnetic phase.

DOI: [10.1103/PhysRevLett.126.016403](https://doi.org/10.1103/PhysRevLett.126.016403)

Rare-earth-based materials are now widely recognized as an ideal playground for exploration of the fascinating physics that develops around a quantum critical point (QCP), a second-order phase transition at zero temperature [1–3]. In Ce-based compounds, such a QCP can be induced by hydrostatic pressure, chemical doping, or a magnetic field, where it typically separates a magnetically ordered state from a nonmagnetic ground state. In spite of numerous experimental investigations of such systems in the vicinity of a QCP, the details of what drives the QCP remain the subject of much theoretical debate. There are currently two fundamentally different theoretical models that attempt to describe the physics of antiferromagnetic (AFM) QCPs in heavy-fermion (HF) materials. The models can be distinguished by whether the Ce 4*f* electrons are localized or itinerant on the either side of a QCP. Here, “itinerant” means that the *f* electrons are fully hybridized with the conduction electrons and therefore contribute to the Fermi surface (FS). The first type of QCP, referred to as a spin-density-wave QCP [4,5], assumes the *f* electrons to be itinerant on both sides of a QCP. In this case, if delocalization of *f* electrons occurs, it occurs inside the magnetic phase. The second type of QCP, known as a Kondo-breakdown QCP [2,6–9], suggests that a transition from itinerant to localized 4*f* electrons occurs precisely at the QCP. Furthermore, the effective masses of the conduction quasiparticles are expected to diverge upon approaching this type of QCP.

Since the FSs with itinerant and localized *f* electrons possess a different size and morphology, the two cases can be easily distinguished experimentally by performing quantum-oscillation measurements such as the de Haas–van Alphen (dHvA) effect. A comparison of the experimental angle-dependent dHvA spectra with results of band-structure calculations, both for localized and itinerant 4*f* electrons, allows us to distinguish between both scenarios. For Ce-based compounds, a comparison can also be made using experimental results obtained on La-based analogs, which serve as *f*-localized references, since the electronic structures of Ce and La differ by only one *f* electron.

CeRhIn<sub>5</sub> is one of the best-studied HF materials. This tetragonal AFM compound with  $T_N = 3.8$  K can be tuned to a QCP by pressure [10–13], chemical substitution [14–16], and magnetic field [17,18]. The pressure-induced QCP in CeRhIn<sub>5</sub> is now considered to be a textbook example of the Kondo-breakdown type. Several dHvA experiments evidence that the *f* electrons of CeRhIn<sub>5</sub> are localized at ambient pressure [19,20], although some of the theoretically predicted dHvA frequencies were not experimentally observed [19]. As the critical pressure for the suppression of antiferromagnetism,  $P_c = 2.3$  GPa, is reached, all dHvA frequencies observed at  $P < P_c$  change discontinuously, signaling an abrupt FS reconstruction as a consequence of the *f*-electron delocalization [21].

In addition, the effective masses diverge at  $P_c$ , further supporting the Kondo-breakdown scenario. A similar discontinuous change of the dHvA frequencies was observed upon substituting Rh by Co in  $\text{CeRh}_{1-x}\text{Co}_x\text{In}_5$  [22]. However, the FS reconstruction does not occur at the critical concentration  $x_c \approx 0.8$ , where the AFM order is suppressed, but deep inside the AFM state at  $x \approx 0.4$ , where the AFM order alters its character and superconductivity emerges to coexist with antiferromagnetism. Furthermore, the effective masses do not diverge here. Thus, the substitution-induced QCP appears to be of the spin-density-wave type.

Recent results obtained at high magnetic fields suggested a unique behavior in  $\text{CeRhIn}_5$ . A field-induced QCP was reported to occur at the critical field  $B_c \approx 50$  T applied along both the  $c$  and  $a$  axes [17,18]. Furthermore, an electronic-nematic phase transition was observed at  $B^*$  and attributed to an in-plane symmetry breaking [23,24]. While  $B^*$  is only weakly temperature and angle dependent, its values obtained from different measurements vary from 27 to 31 T [17,23–27]. Finally, Jiao *et al.* [17,28] reported the emergence of additional dHvA frequencies at  $B^* \approx 30$  T, which was interpreted as a field-induced FS reconstruction associated with the  $f$ -electron delocalization. This result is surprising given that magnetic fields are generally expected to localize  $f$  electrons. This motivated us to thoroughly reexamine the FSs of  $\text{CeRhIn}_5$  at high magnetic fields.

In this Letter, we present the results of high-resolution angle-dependent dHvA measurements on  $\text{CeRhIn}_5$  performed in static fields up to 36 T and pulsed fields up to 70 T. We find that several dHvA frequencies emerge at high fields but are not related to an FS reconstruction. We demonstrate that the  $f$  electrons in  $\text{CeRhIn}_5$  remain localized up to 70 T, well above the critical field to suppress the AFM order.

Figure 1 shows the oscillatory torque after subtracting a nonoscillating background and the corresponding FFTs in  $\text{CeRhIn}_5$  for several magnetic-field orientations  $\theta$ , where  $\theta$  is the angle from the  $c$  toward the  $a$  axis. The FFTs are performed over a field interval mostly above  $B^*$  with a high enough resolution to distinguish various dHvA frequencies. We observed all dHvA frequencies detected in previous low- [19,20,29] and high-field [17,24,28] measurements. In addition, we observed a new, previously undetected dHvA frequency  $\beta_1$ , whose origin will be discussed later in more detail. Almost all of these frequencies are also observed in  $\text{LaRhIn}_5$  [30].

In order to address the question of whether the  $f$  electrons in  $\text{CeRhIn}_5$  are itinerant or localized at high magnetic fields, we performed band-structure calculations [30] for both  $\text{CeRhIn}_5$  with itinerant  $f$  electrons and  $\text{LaRhIn}_5$ . Similar calculations were previously performed for  $\text{CeCoIn}_5$  [19,50] and  $\text{CeIrIn}_5$  [51] with itinerant  $f$  electrons and provided an excellent agreement with experimental results. The calculated FSs, shown in Fig. 2, closely resemble those reported

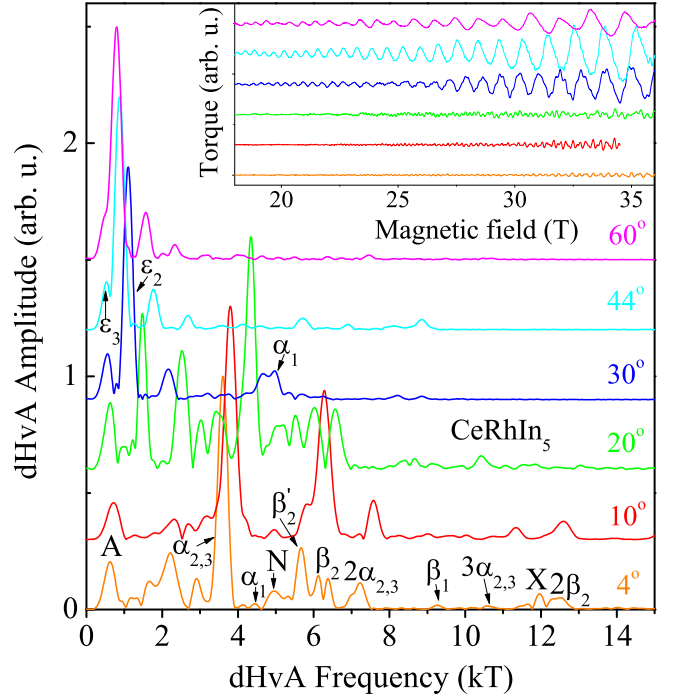


FIG. 1. Fourier spectra of the dHvA oscillations (shown in the inset) of  $\text{CeRhIn}_5$  for a magnetic field applied at various angles,  $\theta$ , from the  $c$  toward the  $a$  axis at  $T = 30$  mK. The curves are shifted vertically for clarity. The FFTs are performed over the field interval from  $B_{\min} = 29$  T to  $B_{\max} = 36$  T, except at  $10^\circ$ , where it is 29–34.5 T (see the inset) due to experimental constraints. All FFTs are normalized to the strongest dHvA spectral peak. An equivalent figure showing the data and FFTs for  $\text{LaRhIn}_5$  is shown in the Supplemental Material [30].

previously [17,19,29,52]. Although there are similarities between the FSs with localized and itinerant  $f$  electrons, several significant morphological differences between the two scenarios are apparent. The morphologies of the quasi-two-dimensional (2D) FS sheets originating from band 15 and giving rise to the  $\alpha$  orbits are almost identical. Only the orbit size is different. There is, however, an additional three-dimensional (3D) FS sheet in the itinerant scenario. The FS sheets originating from band 13 are considerably different in the localized and itinerant cases. The complicated crosslike sheet giving rise to the  $\epsilon$  orbits in the localized case is replaced by two small ellipsoidal pockets in the itinerant scenario. The most essential difference, however, is the morphology of the FS sheets originating from the electron band 14. In the localized case, a quasi-2D sheet gives rise to the orbits  $\beta_1$  (belly) and  $\beta_2$  (neck). In the itinerant scenario, on the contrary, this sheet is more 3D with a larger  $\beta_1$  orbit that is present over a more limited angular range and an entirely missing neck orbit  $\beta_2$ . The latter is replaced by a much smaller hole orbit  $\beta_2^*$ , which exists at very small angles only. This difference alone is sufficient to decide which of the calculated FSs yields a better agreement with the experimental results.

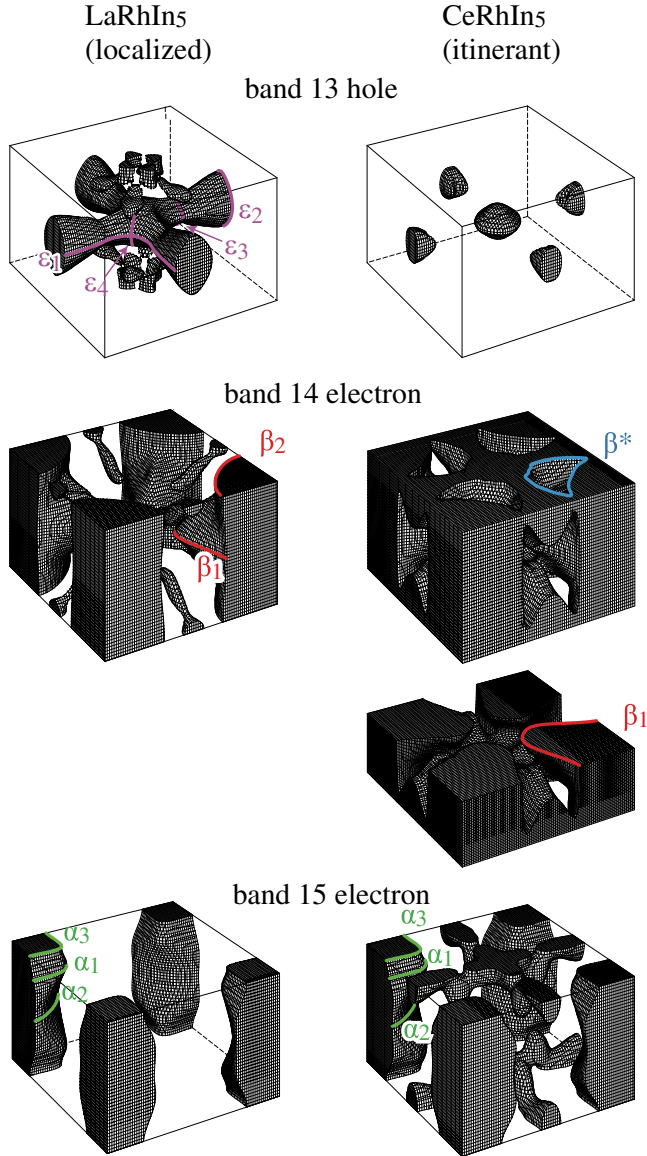


FIG. 2. Calculated FSs with localized (left) and itinerant (right)  $f$  electrons. Solid lines indicate some extremal cross sections as discussed in the text.

With this in mind, we will now compare the experimentally obtained angular dependence of the dHvA frequencies in CeRhIn<sub>5</sub> to the band-structure calculations for both localized [Fig. 3(a)] and itinerant [Fig. 3(b)]  $f$  electrons. For this comparison, the dHvA frequencies were extracted from FFTs, such as shown in Fig. 1, performed over the field range 29–36 T [53] ( $B_{\text{avg}} = 32.12$  T [54]).

There is excellent agreement between the experimentally observed branches  $\alpha_{2,3}$ ,  $\alpha_1$ ,  $\beta_2$ , and  $\beta_1$  and their counterparts calculated for localized  $f$  electrons [Fig. 3(a)]. These branches originate from the quasi-2D FS sheets from bands 14 and 15. The experimentally observed branches  $\varepsilon_2$  and  $\varepsilon_3$  also agree very well with the  $f$ -localized calculations. These branches originate from the crosslike FS sheet from band 13. The branch X is observed only at small angles close to the  $c$  axis, and it does not seem to correspond to any calculated extremal area. Neither do the branches  $\beta'_2$  and  $N$  correspond to any calculated branch. These frequencies will be discussed later in more detail.

On the other hand, there is a clear disagreement of the experimental data with band-structure calculations assuming itinerant  $f$  electrons [Fig. 3(b)]. The most significant signature of this disagreement is the presence of the  $\beta_2$  branch, which is supposed to be completely absent in the itinerant scenario. This branch was also observed in previous high-field dHvA [17,28] and magnetostriction [24] measurements. In measurements under high pressure, this frequency disappears above  $P_c$ , where the  $f$  electrons become itinerant [21]. Furthermore, the experimentally observed  $\alpha_{2,3}$ ,  $\alpha_1$ , and  $\beta_1$  branches lie far below those calculated for the itinerant case. In previous high-field dHvA measurements performed with a magnetic field only along the  $c$  axis, the frequencies  $N$  and  $\beta'_2$  were interpreted as  $\alpha_2$  and  $\alpha_1$  of the  $f$ -itinerant model [17]. However, their angular dependence is clearly different from that suggested by the calculations. Similarly, the experimentally observed branch X was interpreted as the  $\beta_1$  branch of the itinerant scenario [17]. This frequency indeed agrees with calculated

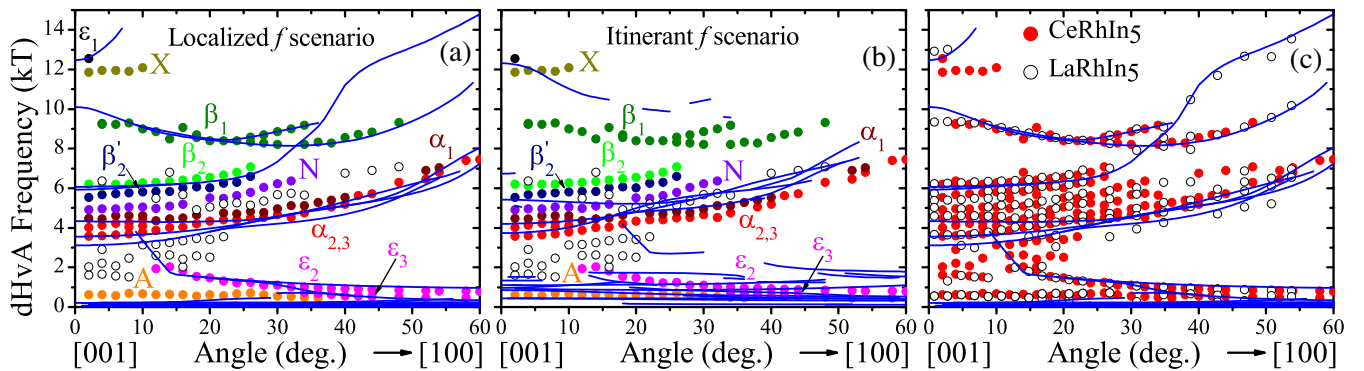


FIG. 3. Angular dependence of the experimentally observed dHvA frequencies in CeRhIn<sub>5</sub> together with results of band-structure calculations (solid lines) within localized (a) and itinerant (b) scenarios, and with the experimentally observed dHvA frequencies in LaRhIn<sub>5</sub> (open circles) (c). In the latter case, the band-structure calculations for localized  $f$  electrons are also shown.

$\beta_1$  values at small angles close to the  $c$  axis. The positive curvature of this branch, however, is inconsistent with the negative curvature of the calculated  $\beta_1$  branch.

Finally, in Fig. 3(c), we compare the angular dependence of the experimentally observed dHvA frequencies in CeRhIn<sub>5</sub> and LaRhIn<sub>5</sub>. The dHvA frequencies of the latter compound were also obtained from high-field ranges up to the available  $B_{\max}$  [30]. The excellent agreement of the experimentally measured dHvA frequencies observed in CeRhIn<sub>5</sub> and LaRhIn<sub>5</sub> over the whole angular range is an especially strong confirmation that the  $f$  electrons, which are localized at low fields [19], remain so even in fields higher than  $B^*$ . Furthermore, the dHvA frequencies observed in CeRhIn<sub>5</sub> at high fields do not match those observed above the critical pressure [30].

Figures 1 to 3 convincingly demonstrate that the Ce  $f$  electrons are localized up to 36 T. That this situation persists up to still higher fields is evidenced by our pulsed-field measurements, shown in Fig. 4(a). The corresponding FFT spectra obtained over a moving  $1/B$  window are shown in Fig. 4(b). Due to the much higher temperature,  $T = 620$  mK, of the pulsed-field measurements, some of the additional dHvA frequencies, such as  $N$ ,  $\beta_1$ , and  $X$ , emerge at higher fields as compared to our lower temperature static-field results, an example of which is shown in Fig. 4(c). Contrary to the previous report [17], some of these frequencies emerge well below  $B^*$ , as can be seen in Fig. 4(b) and (c). We have not observed any frequency shift or the emergence of new frequencies at either  $B^*$  or  $B_c$  (inset of Fig. 4). Importantly, the  $\beta_2$  frequency is still present above  $B_c \simeq 50$  T. Furthermore, the effective masses remain finite in the immediate vicinity of  $B_c$  [30]. This suggests that the  $f$  electrons remain localized when the AFM order is suppressed by a magnetic field. The same conclusion was drawn for CeIn<sub>3</sub>, for which the AFM order is also suppressed at a very high field of about 60 T [55].

We will now discuss the origin of the additional dHvA frequencies, such as  $\beta'_2$ ,  $N$ ,  $\beta_1$ , and  $X$ , which emerge only at high fields. The frequency  $\beta_1$  originates from the belly orbit of the electron band 14 (Fig. 2). Both the frequency itself and its angular dependence are in excellent agreement with the  $f$ -localized calculations [Fig. 3(a)]. This branch was not observed in any of the previous measurements. This is not surprising given that this orbit is strongly affected by the modification of the Brillouin zone in the AFM state [30]. In addition, the corresponding effective mass is strongly enhanced,  $m^* \simeq 12m_0$  [30]. The frequencies  $\beta'_2$  and  $N$  do not seem to correspond to any calculated branch within either the localized or itinerant model. It is, however, apparent that  $\beta'_2$  follows the angular variation of  $\beta_2$  with a small and almost constant offset (Fig. 3). Remarkably, this offset  $\sim 0.6$  kT, corresponds to the frequency  $A$ , which is almost angle independent. This suggests that  $\beta'_2$  originates from the magnetic breakdown between  $\beta_2$  and  $A$ , i.e.,

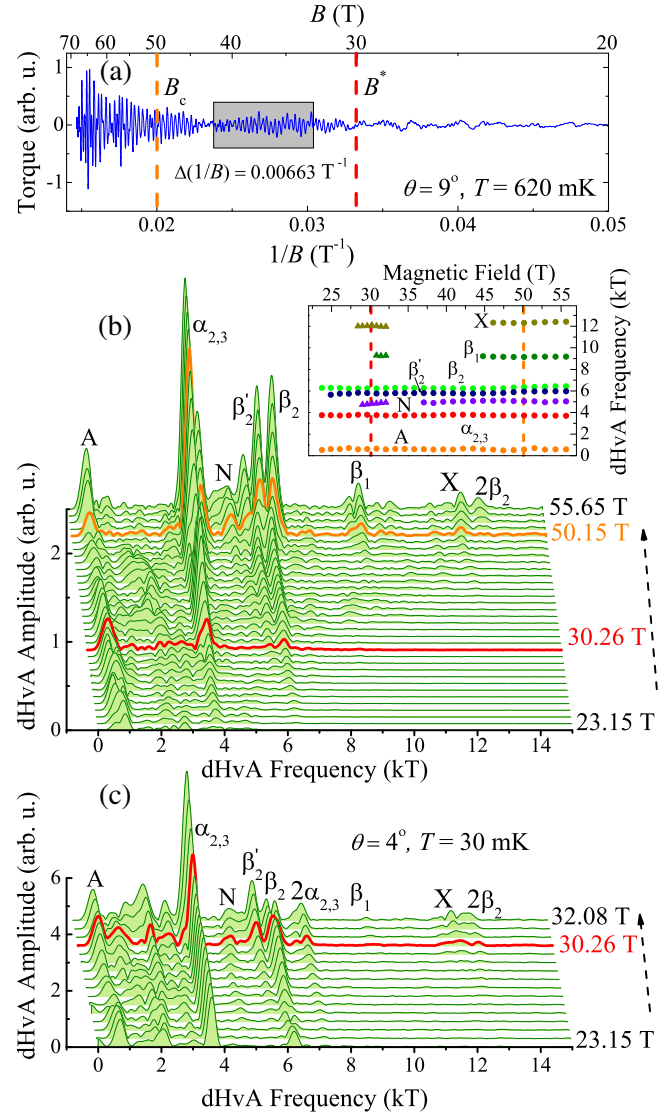


FIG. 4. dHvA oscillations in CeRhIn<sub>5</sub> (a) in pulsed magnetic fields applied at  $9^\circ$  from the  $c$  axis. (b) FFT spectra of the oscillations from (a) obtained over the same  $1/B$  range, shown by the rectangle in (a). For the bottom curve, the range is from  $B_{\min} = 21.5$  T to  $B_{\max} = 25.07$  T ( $B_{\text{avg}} = 23.15$  T). For each successive curve,  $B_{\min}$  is increased by 0.5 T up to 29 T and by 1 T from there on. The inset shows the evolution of the dHvA frequencies with  $B$  obtained from pulsed (circles) and static (triangles) field measurements. (c) FFT spectra of the static-field dHvA oscillations, shown in Fig. 1, with  $B$  at  $4^\circ$  from the  $c$  axis. The  $1/B$  range and the range for the bottom curve are the same as in (b). For each successive curve,  $B_{\min}$  is increased by 0.5 T. The curves in (b) and (c) are shifted for clarity.

$\beta'_2 = \beta_2 - A$ , assuming that  $A$  corresponds to a hole pocket. The exact origin of the frequencies  $N$  and  $X$  is unclear at present. Notably, the  $\beta'_2$  and  $N$  branches also emerge in LaRhIn<sub>5</sub> only at high fields [see Fig. 3(c)] [30], suggesting that they originate from magnetic-breakdown orbits. The frequency  $X$  is the only one that is not observed in LaRhIn<sub>5</sub>. It is, therefore, less likely that this frequency originates

from a magnetic breakdown. Its emergence at high fields, although progressive [30], could be due to a minor FS reconstruction, such as a Lifshitz transition of a spin-split band, similar to what was observed in CeIrIn<sub>5</sub> [56] and YbRh<sub>2</sub>Si<sub>2</sub> [57]. We emphasize that even if this is the case, the  $f$  electrons remain localized above 30 T, as is evidenced by the presence of the  $\beta_1$  and  $\beta_2$  frequencies and the very close match between the LaRhIn<sub>5</sub> and the CeRhIn<sub>5</sub> data.

In summary, we performed high-field dHvA measurements on CeRhIn<sub>5</sub> and LaRhIn<sub>5</sub>. In CeRhIn<sub>5</sub>, several additional dHvA frequencies emerge above certain threshold fields. In particular, we observed the previously undetected, thermodynamically important  $\beta_1$  branch predicted by the  $f$ -localized band-structure calculations. Almost all of the dHvA frequencies observed in CeRhIn<sub>5</sub> are also present in LaRhIn<sub>5</sub>. In addition, their angular dependence is identical in the two compounds. The presence and angle dependence of the observed dHvA frequencies are well accounted for by band-structure calculations with localized  $f$  electrons, indicating that the  $f$  electrons of CeRhIn<sub>5</sub> remain localized not only above  $B^* \approx 30$  T but also above  $B_c \approx 50$  T. We emphasize that delocalization of the Ce  $f$  electron at high magnetic field would change the whole FS from the localized to the itinerant FS that we show in Fig. 2. Continued observation of the  $\beta_2$  branch at the highest magnetic fields is clear evidence of that the Ce  $f$  electron remains localized over the full magnetic field range that we have explored.

It was previously reported that the  $f$  electrons also remain localized in CeIn<sub>3</sub> above its critical field  $B_c \approx 60$  T [55]. Whereas CeIn<sub>3</sub> is an isotropic HF compound with an almost spheroidal FS, CeRhIn<sub>5</sub> is a prototypical example of a strongly anisotropic material with quasi-2D FSs. The continued localization of the  $f$  electrons well above  $B_c$  in both compounds is not consistent with either of the two existing theoretical models of AFM QCPs. This implies that magnetic field, which itself tends to localize  $f$  electrons, should be treated differently from such control parameters as pressure or chemical doping.

We thank H. Shishido for sharing with us the high-pressure dHvA data and R. Settai for sharing with us the results obtained in CeCoIn<sub>5</sub>. We acknowledge the support of the LNCMI-CNRS, the HLD-HZDR, and the HFML-RU, members of the European Magnetic Field Laboratory (EMFL), the ANR-DFG grant ‘‘Fermi-NESst,’’ the DFG through the excellence cluster *ct.qmat* (EXC 2147, Project ID 39085490), and JSPS KAKENHI Grant Nos. JP15H05882, JP15H05884, JP15H05886, and JP15K21732 (J-Physics).

---

\*Corresponding author.  
ilya.sheikin@lncmi.cnrs.fr

- <sup>†</sup>Present address: IRIG/DEPHY/MEM-MDN, CEA-Grenoble, 17 Avenue des Martyrs, 38000 Grenoble, France.
- [1] P. Gegenwart, Q. Si, and F. Steglich, Quantum criticality in heavy-fermion metals, *Nat. Phys.* **4**, 186 (2008).
  - [2] Q. Si, S. Rabello, K. Ingersent, and J. L. Smith, Locally critical quantum phase transitions in strongly correlated metals, *Nature (London)* **413**, 804 (2001).
  - [3] T. Senthil, Deconfined quantum critical points, *Science* **303**, 1490 (2004).
  - [4] J. A. Hertz, Quantum critical phenomena, *Phys. Rev. B* **14**, 1165 (1976).
  - [5] A. J. Millis, Effect of a nonzero temperature on quantum critical points in itinerant fermion systems, *Phys. Rev. B* **48**, 7183 (1993).
  - [6] S. Paschen, T. Lhmann, S. Wirth, P. Gegenwart, O. Trovarelli, C. Geibel, F. Steglich, P. Coleman, and Q. Si, Hall-effect evolution across a heavy-fermion quantum critical point, *Nature (London)* **432**, 881 (2004).
  - [7] P. Coleman, C. Pépin, Q. Si, and R. Ramazashvili, How do Fermi liquids get heavy and die?, *J. Phys. Condens. Matter* **13**, R723 (2001).
  - [8] P. Gegenwart, T. Westerkamp, C. Krellner, Y. Tokiwa, S. Paschen, C. Geibel, F. Steglich, E. Abrahams, and Q. Si, Multiple energy scales at a quantum critical point, *Science* **315**, 969 (2007).
  - [9] S. Friedemann, N. Oeschler, S. Wirth, C. Krellner, C. Geibel, F. Steglich, S. Paschen, S. Kirchner, and Q. Si, Fermi-surface collapse and dynamical scaling near a quantum-critical point, *Proc. Natl. Acad. Sci. U.S.A.* **107**, 14547 (2010).
  - [10] H. Hegger, C. Petrovic, E. G. Moshopoulou, M. F. Hundley, J. L. Sarrao, Z. Fisk, and J. D. Thompson, Pressure-Induced Superconductivity in Quasi-2D CeRhIn<sub>5</sub>, *Phys. Rev. Lett.* **84**, 4986 (2000).
  - [11] T. Mito, S. Kawasaki, Y. Kawasaki, G. Q. Zheng, Y. Kitaoka, D. Aoki, Y. Haga, and Y. Ōnuki, Coexistence of Antiferromagnetism and Superconductivity near the Quantum Criticality of the Heavy-Fermion Compound CeRhIn<sub>5</sub>, *Phys. Rev. Lett.* **90**, 077004 (2003).
  - [12] G. Knebel, D. Aoki, D. Braithwaite, B. Salce, and J. Flouquet, Coexistence of antiferromagnetism and superconductivity in CeRhIn<sub>5</sub> under high pressure and magnetic field, *Phys. Rev. B* **74**, 020501(R) (2006).
  - [13] T. Park, F. Ronning, H. Q. Yuan, M. B. Salamon, R. Movshovich, J. L. Sarrao, and J. D. Thompson, Hidden magnetism and quantum criticality in the heavy fermion superconductor CeRhIn<sub>5</sub>, *Nature (London)* **440**, 65 (2006).
  - [14] P. G. Pagliuso, C. Petrovic, R. Movshovich, D. Hall, M. F. Hundley, J. L. Sarrao, J. D. Thompson, and Z. Fisk, Coexistence of magnetism and superconductivity in CeRh<sub>1-x</sub>Ir<sub>x</sub>In<sub>5</sub>, *Phys. Rev. B* **64**, 100503(R) (2001).
  - [15] V. S. Zapf, E. J. Freeman, E. D. Bauer, J. Petricka, C. Sirvent, N. A. Frederick, R. P. Dickey, and M. B. Maple, Coexistence of superconductivity and antiferromagnetism in CeRh<sub>1-x</sub>Co<sub>x</sub>In<sub>5</sub>, *Phys. Rev. B* **65**, 014506 (2001).
  - [16] E. Bauer, D. Mixson, F. Ronning, N. Hur, R. Movshovich, J. Thompson, J. Sarrao, M. Hundley, P. Tobash, and S. Bobev, Antiferromagnetic quantum critical point in CeRhIn<sub>5-x</sub>Sn<sub>x</sub>, *Physica (Amsterdam)* **378–380B**, 142 (2006).

- [17] L. Jiao, Y. Chen, Y. Kohama, D. Graf, E. D. Bauer, J. Singleton, J.-X. Zhu, Z. Weng, G. Pang, T. Shang, J. Zhang, H.-O. Lee, T. Park, M. Jaime, J. D. Thompson, F. Steglich, Q. Si, and H. Q. Yuan, Fermi surface reconstruction and multiple quantum phase transitions in the antiferromagnet CeRhIn<sub>5</sub>, *Proc. Natl. Acad. Sci. U.S.A.* **112**, 673 (2015).
- [18] L. Jiao, M. Smidman, Y. Kohama, Z. S. Wang, D. Graf, Z. F. Weng, Y. J. Zhang, A. Matsuo, E. D. Bauer, H. Lee, S. Kirchner, J. Singleton, K. Kindo, J. Wosnitza, F. Steglich, J. D. Thompson, and H. Q. Yuan, Enhancement of the effective mass at high magnetic fields in CeRhIn<sub>5</sub>, *Phys. Rev. B* **99**, 045127 (2019).
- [19] H. Shishido, R. Settai, D. Aoki, S. Ikeda, H. Nakawaki, N. Nakamura, T. Iizuka, Y. Inada, K. Sugiyama, T. Takeuchi, K. Kindo, T. C. Kobayashi, Y. Haga, H. Harima, Y. Aoki, T. Namiki, H. Sato, and Y. Ōnuki, Fermi surface, magnetic and superconducting properties of LaRhIn<sub>5</sub> and CeTlIn<sub>5</sub> (T: Co, Rh and Ir), *J. Phys. Soc. Jpn.* **71**, 162 (2002).
- [20] N. Harrison, U. Alver, R. G. Goodrich, I. Vekhter, J. L. Sarrao, P. G. Pagliuso, N. O. Moreno, L. Balicas, Z. Fisk, D. Hall, R. T. Macaluso, and J. Y. Chan, *4f*-Electron Localization in Ce<sub>x</sub>La<sub>1-x</sub>MIn<sub>5</sub> with M = Co, Rh, or Ir, *Phys. Rev. Lett.* **93**, 186405 (2004).
- [21] H. Shishido, R. Settai, H. Harima, and Y. Ōnuki, A drastic change of the fermi surface at a critical pressure in CeRhIn<sub>5</sub>: dHvA study under pressure, *J. Phys. Soc. Jpn.* **74**, 1103 (2005).
- [22] S. K. Goh, J. Paglione, M. Sutherland, E. C. T. O'Farrell, C. Bergemann, T. A. Sayles, and M. B. Maple, Fermi-Surface Reconstruction in CeRh<sub>1-x</sub>Co<sub>x</sub>In<sub>5</sub>, *Phys. Rev. Lett.* **101**, 056402 (2008).
- [23] F. Ronning, T. Helm, K. R. Shirer, M. D. Bachmann, L. Balicas, M. K. Chan, B. J. Ramshaw, R. D. McDonald, F. F. Balakirev, M. Jaime, E. D. Bauer, and P. J. W. Moll, Electronic in-plane symmetry breaking at field-tuned quantum criticality in CeRhIn<sub>5</sub>, *Nature (London)* **548**, 313 (2017).
- [24] P. F. S. Rosa, S. M. Thomas, F. F. Balakirev, E. D. Bauer, R. M. Fernandes, J. D. Thompson, F. Ronning, and M. Jaime, Enhanced Hybridization Sets the Stage for Electronic Nematicity in CeRhIn<sub>5</sub>, *Phys. Rev. Lett.* **122**, 016402 (2019).
- [25] P. J. W. Moll, B. Zeng, L. Balicas, S. Galeski, F. F. Balakirev, E. D. Bauer, and F. Ronning, Field-induced density wave in the heavy-fermion compound CeRhIn<sub>5</sub>, *Nat. Commun.* **6**, 6663 (2015).
- [26] G. G. Lesseux, H. Sakai, T. Hattori, Y. Tokunaga, S. Kambe, P. L. Kuhns, A. P. Reyes, J. D. Thompson, P. G. Pagliuso, and R. R. Urbano, Orbitaly defined field-induced electronic state in a Kondo lattice, *Phys. Rev. B* **101**, 165111 (2020).
- [27] R. Kurihara, A. Miyake, M. Tokunaga, Y. Hirose, and R. Settai, High-field ultrasonic study of quadrupole ordering and crystal symmetry breaking in CeRhIn<sub>5</sub>, *Phys. Rev. B* **101**, 155125 (2020).
- [28] L. Jiao, Z. F. Weng, M. Smidman, D. Graf, J. Singleton, E. D. Bauer, J. D. Thompson, and H. Q. Yuan, Magnetic field-induced Fermi surface reconstruction and quantum criticality in CeRhIn<sub>5</sub>, *Philos. Mag.* **97**, 3446 (2017).
- [29] D. Hall, E. Palm, T. Murphy, S. W. Tozer, C. Petrovic, E. Miller-Ricci, L. Peabody, C. Q. H. Li, U. Alver, R. G. Goodrich, J. L. Sarrao, P. G. Pagliuso, J. M. Wills, and Z. Fisk, Electronic structure of CeRhIn<sub>5</sub>: de Haas–van Alphen and energy band calculations, *Phys. Rev. B* **64**, 064506 (2001).
- [30] See Supplemental Material, which includes Refs. [31–49], at <http://link.aps.org/supplemental/10.1103/PhysRevLett.126.016403> for the experimental details, dHvA oscillations in LaRhIn<sub>5</sub>, band-structure calculations, effective masses, angle dependence of the metamagnetic transition, and field dependence of the oscillatory amplitudes of the X and β<sub>1</sub> branches, as well as a comparison of the dHvA frequencies in CeRhIn<sub>5</sub> at high magnetic fields and under high pressure.
- [31] O. Gunnarsson and B. I. Lundqvist, Exchange and correlation in atoms, molecules, and solids by the spin-density-functional formalism, *Phys. Rev. B* **13**, 4274 (1976).
- [32] Y. Haga (private communication).
- [33] J. Thompson, R. Movshovich, Z. Fisk, F. Bouquet, N. Curro, R. Fisher, P. Hammel, H. Hegger, M. Hundley, M. Jaime, P. Pagliuso, C. Petrovic, N. Phillips, and J. Sarrao, Superconductivity and magnetism in a new class of heavy-fermion materials, *J. Magn. Magn. Mater.* **226–230**, 5 (2001).
- [34] E. Moshopoulou, Z. Fisk, J. Sarrao, and J. Thompson, Crystal growth and intergrowth structure of the new heavy fermion materials CeIrIn<sub>5</sub> and CeRhIn<sub>5</sub>, *J. Solid State Chem.* **158**, 25 (2001).
- [35] E. Moshopoulou, J. Sarrao, P. Pagliuso, N. Moreno, J. Thompson, Z. Fisk, and R. Ibberson, Comparison of the crystal structure of the heavy-fermion materials CeCoIn<sub>5</sub>, CeRhIn<sub>5</sub> and CeIrIn<sub>5</sub>, *Appl. Phys. A* **74**, s895 (2002).
- [36] D. D. Koelling and B. N. Harmon, A technique for relativistic spin-polarised calculations, *J. Phys. C* **10**, 3107 (1977).
- [37] D. Shoenberg, *Magnetic Oscillations in Metals* (Cambridge University Press, Cambridge, England, 1984).
- [38] W. Joss, J. M. van Ruitenbeek, G. W. Crabtree, J. L. Tholence, A. P. J. van Deursen, and Z. Fisk, Observation of the Magnetic Field Dependence of the Cyclotron Mass in the Kondo Lattice CeB<sub>6</sub>, *Phys. Rev. Lett.* **59**, 1609 (1987).
- [39] N. Harrison, P. Meeson, P. A. Probst, and M. Springford, Quasiparticle and thermodynamic mass in the heavy-fermion system CeB<sub>6</sub>, *J. Phys. Condens. Matter* **5**, 7435 (1993).
- [40] E. Haanappel, L. Pricopi, A. Demuer, and P. Lejay, Field-dependent cyclotron mass of CeAl<sub>2</sub>, *Physica (Amsterdam)* **259–261B**, 1081 (1999).
- [41] L. Pricopi, E. Haanappel, S. Askénazy, N. Harrison, M. Bennett, P. Lejay, A. Demuer, and G. Lapertot, de Haas–van Alphen studies of the heavy fermions CeAl<sub>2</sub> and CeRu<sub>2</sub>Si<sub>2</sub>, *Physica (Amsterdam)* **294–295B**, 276 (2001).
- [42] W. Bao, P. G. Pagliuso, J. L. Sarrao, J. D. Thompson, Z. Fisk, J. W. Lynn, and R. W. Erwin, Incommensurate magnetic structure of CeRhIn<sub>5</sub>, *Phys. Rev. B* **62**, R14621 (2000).
- [43] D. M. Fobes, E. D. Bauer, J. D. Thompson, A. Sazonov, V. Hutanu, S. Zhang, F. Ronning, and M. Janoschek, Low temperature magnetic structure of CeRhIn<sub>5</sub> by neutron diffraction on absorption-optimized samples, *J. Phys. Condens. Matter* **29**, 17LT01 (2017).
- [44] A. L. Cornelius, P. G. Pagliuso, M. F. Hundley, and J. L. Sarrao, Field-induced magnetic transitions in the quasi-two-

- dimensional heavy-fermion antiferromagnets  $Ce_nRhIn_{3n+2}$  ( $n = 1$  or  $2$ ), *Phys. Rev. B* **64**, 144411 (2001).
- [45] V. F. Correa, W. E. Okraku, J. B. Betts, A. Migliori, J. L. Sarrao, and A. H. Lacerda, High-magnetic-field thermal expansion and elastic properties of  $CeRhIn_5$ , *Phys. Rev. B* **72**, 012407 (2005).
- [46] S. Raymond, E. Ressouche, G. Knebel, D. Aoki, and J. Flouquet, Magnetic structure of  $CeRhIn_5$  under magnetic field, *J. Phys. Condens. Matter* **19**, 242204 (2007).
- [47] D. M. Fobes, S. Zhang, S.-Z. Lin, P. Das, N. J. Ghimire, E. D. Bauer, J. D. Thompson, L. W. Harriger, G. Ehlers, A. Podlesnyak, R. I. Bewley, A. Sazonov, V. Hutanu, F. Ronning, C. D. Batista, and M. Janoschek, Tunable emergent heterostructures in a prototypical correlated metal, *Nat. Phys.* **14**, 456 (2018).
- [48] T. Kanda, K. Arashima, Y. Hirose, R. Settai, K. Matsui, T. Nomura, Y. Kohama, and Y. Ihara, Symmetry lowering on the field-induced commensurate phase in  $CeRhIn_5$ , *J. Phys. Soc. Jpn.* **89**, 094709 (2020).
- [49] D. Hall, E. C. Palm, T. P. Murphy, S. W. Tozer, Z. Fisk, U. Alver, R. G. Goodrich, J. L. Sarrao, P. G. Pagliuso, and T. Ebihara, Fermi surface of the heavy-fermion superconductor  $CeCoIn_5$ : The de Haas–van Alphen effect in the normal state, *Phys. Rev. B* **64**, 212508 (2001).
- [50] R. Settai, H. Shishido, S. Ikeda, Y. Murakawa, M. Nakashima, D. Aoki, Y. Haga, H. Harima, and Y. Onuki, Quasi-two-dimensional Fermi surfaces and the de Haas-van Alphen oscillation in both the normal and superconducting mixed states of  $CeCoIn_5$ , *J. Phys. Condens. Matter* **13**, L627 (2001).
- [51] Y. Haga, Y. Inada, H. Harima, K. Oikawa, M. Murakawa, H. Nakawaki, Y. Tokiwa, D. Aoki, H. Shishido, S. Ikeda, N. Watanabe, and Y. Onuki, Quasi-two-dimensional Fermi surfaces of the heavy fermion superconductor  $CeIrIn_5$ , *Phys. Rev. B* **63**, 060503(R) (2001).
- [52] S. Elgazzar, I. Opahle, R. Hayn, and P. M. Oppeneer, Calculated de Haas–van Alphen quantities of  $CeMIn_5$  ( $M = Co, Rh,$  and  $Ir$ ) compounds, *Phys. Rev. B* **69**, 214510 (2004).
- [53] This range, mostly above  $B^*$ , was chosen to provide a high enough resolution to distinguish close dHVA frequencies. A small variation of this range does not alter the results.
- [54] Throughout this Letter, the average field  $B_{\text{avg}}$  of a field interval from  $B_{\text{min}}$  to  $B_{\text{max}}$  is defined as the reciprocal average, i.e.,  $1/B_{\text{avg}} = 1/2(1/B_{\text{min}} + 1/B_{\text{max}})$ .
- [55] N. Harrison, S. E. Sebastian, C. H. Mielke, A. Paris, M. J. Gordon, C. A. Swenson, D. G. Rickel, M. D. Pacheco, P. F. Ruminer, J. B. Schillig, J. R. Sims, A. H. Lacerda, M.-T. Suzuki, H. Harima, and T. Ebihara, Fermi Surface of  $CeIn_3$  above the Néel Critical Field, *Phys. Rev. Lett.* **99**, 056401 (2007).
- [56] D. Aoki, G. Seyfarth, A. Pourret, A. Gourgout, A. McCollam, J. A. N. Bruin, Y. Krupko, and I. Sheikin, Field-Induced Lifshitz Transition without Metamagnetism in  $CeIrIn_5$ , *Phys. Rev. Lett.* **116**, 037202 (2016).
- [57] P. M. C. Rourke, A. McCollam, G. Lapertot, G. Knebel, J. Flouquet, and S. R. Julian, Magnetic-Field Dependence of the  $YbRh_2Si_2$  Fermi Surface, *Phys. Rev. Lett.* **101**, 237205 (2008).